Volume 3
Number 11
November 2025
Pages 4837–5396

RSC Sustainability

rsc.li/rscsus

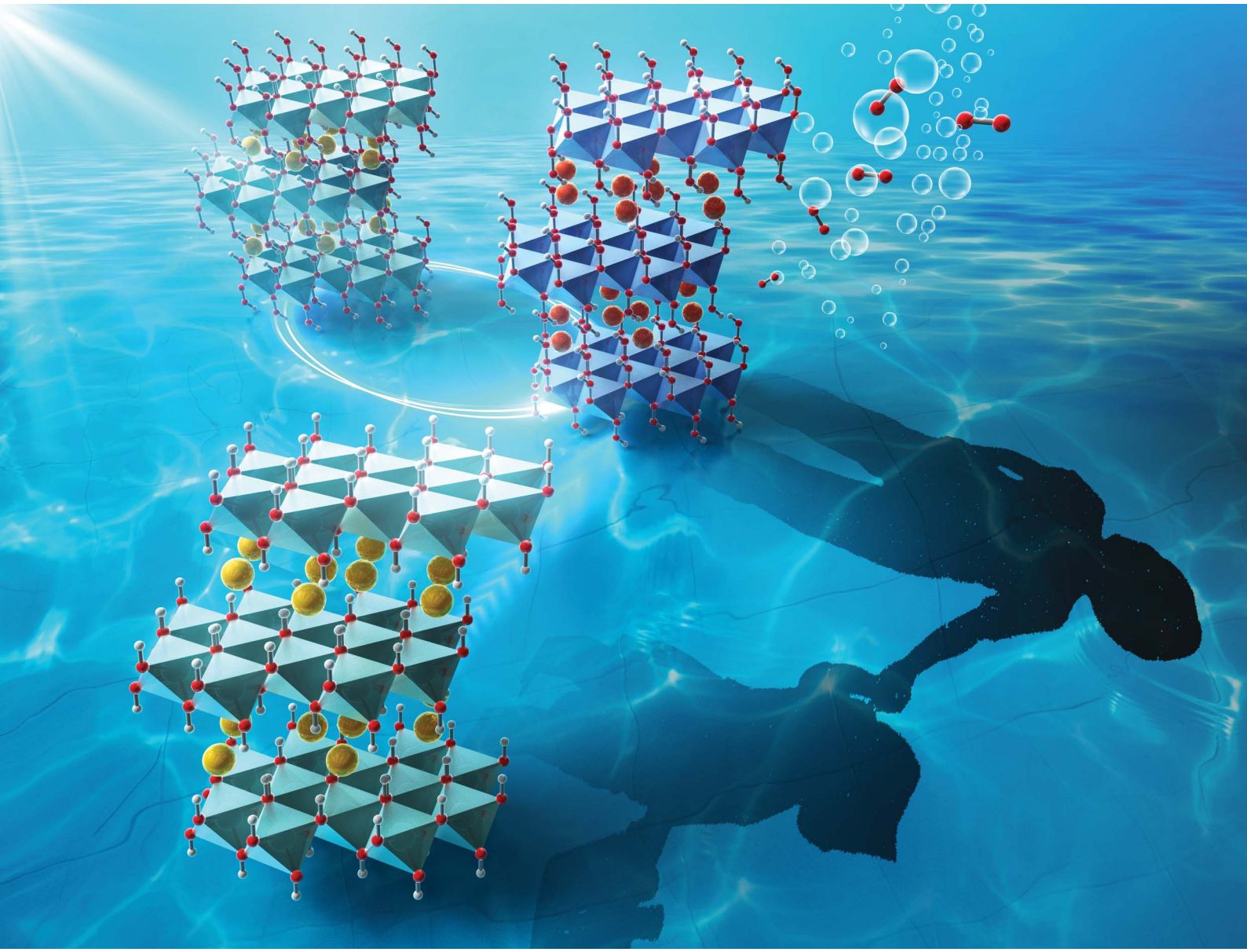

ISSN 2753-8125

ROYAL SOCIETY OF CHEMISTRY

PAPER

Mitsuharu Chisaka *et al.*

Reversible valence states with irreversible crystal structures of NiFe layered double hydroxide catalysts: surface stability during the oxygen evolution reaction

RSC Sustainability

ROYAL SOCIETY OF CHEMISTRY

PAPER

View Article Online
View Journal | View Issue

Cite this: *RSC Sustainability*, 2025, **3**, 5128

Reversible valence states with irreversible crystal structures of NiFe layered double hydroxide catalysts: surface stability during the oxygen evolution reaction

Taiyo Fukui,†[a] Takashi Itoh,†[b] Mitsuharu Chisaka *[a] and Toshiyuki Abe [c]

Received 9th July 2025
Accepted 13th August 2025

DOI: 10.1039/d5su00578g

rsc.li/rscsus

Stability is crucial in catalysis, and contrasting results have been reported for the most active platinum-group-metal free oxygen evolution reaction (OER) catalyst, nickel–iron layered double hydroxide (NiFe-LDH). In addition, different active valence states have been reported. In this study, stable valence/chemical states on the surface of stable NiFe-LDH were investigated using a combination of *in situ* visible Raman spectroscopy, *ex situ* visible/ultraviolet (UV) Raman spectroscopy, and *ex situ* X-ray photoelectron spectroscopy (XPS). A recently reported coprecipitation method for preparing stable NiFe-LDH without doping or intercalation of specific anions was applied to nickel foam (NF) in this study, and surface stability was investigated using chronopotentiometry (CP) for 24 h. The surface of NiFe-LDH was converted from hydroxide into oxyhydroxide, but its initial stable valence states, Ni^{2+} and Fe^{3+}, were retained after a stable operation period.

Sustainability spotlight

Sustainable approaches that meet the increasing demand for electricity while maximizing the use of sustainable energy sources, such as the sun and wind, are required. Electrochemical alkaline water splitting into hydrogen and oxygen is one of the promising solutions to convert these fluctuating energy sources into hydrogen fuels, which can be used at the point of consumption. However, the slow kinetics of the oxygen evolution reaction require scarce and expensive IrO_2 catalysts, which hinder the widespread use of this approach. In this work, stable surface valence/chemical states of the most active Ir-free oxygen evolution catalyst, nickel–iron layered double hydroxides, were revealed. This work aligns with the following UN sustainable development goals: affordable and clean energy (SDG 7); industry, innovation, and infrastructure (SDG 9); and climate action (SDG 13).

Introduction

The trend in energy consumption is driven by the economic and population growth rates in a counrty or a region; it will decrease in some developed countries. However, electricity consumption is expected to increase continuously worldwide. The global demand for electricity is predicted to increase from 22 536 terawatt hour in 2020 to 35 407 terawatt hour in 2040.[1] Sustainable approaches that satisfy the increasing demand for electricity must optimize the use of sustainable energy sources such as the sun and wind. Electrochemical alkaline water splitting into hydrogen (H_2) and oxygen (O_2), also termed alkaline water electrolysis, is a promising solution to convert fluctuating energy sources into H_2 fuels that can be used at the point of consumption. Platinum (Pt) and iridium oxide (IrO_2) are currently the best catalysts for hydrogen evolution reactions (HERs) and oxygen evolution reactions (OERs), respectively. However, Ir is a highly expensive and scarce metal, with a 2021–2023 price approximately five times higher than that of Pt.[2] In addition, slower kinetics of OERs than HERs are the primary sources requiring high voltages for commercial alkaline water electrolyzers at 1.7–1.9 V. These voltages are substantially higher than the theoretical requirement of 1.23 V.[3] Therefore, significant efforts have been dedicated toward developing earth-abundant alternatives to Ir-based OER catalysts.

Nickel–iron layered double hydroxides (NiFe-LDHs) are the most widely studied non-Ir OER catalyst because of their highest OER activity among reported catalysts.[4] They consist of positively charged hydroxide layers and hydrated intercalated anions with the formula $[Ni_{1-x}^{2+}Fe_x^{3+}(OH)_2]^{x+}(A^{n-})_{x/n}\cdot y(H_2O)$, where A^{n-} is the interlayer anion, typically CO_3^{2-} for the as-prepared LDHs; the origin is dissolved carbon dioxide gas from the air moisture.[5] Charge imbalances resulting from the substitution of Ni^{2+} with Fe^{3+} in $Ni(OH)_2$ are compensated upon

[a]*Department of Sustainable Energy, Hirosaki University, 3 Bunkyo-cho, Hirosaki, Aomori 036-8561, Japan. E-mail: chisaka@hirosaki-u.ac.jp*

[b]*Frontier Research Institute for Interdisciplinary Sciences (FRIS), Tohoku University, 6-3 Aramaki-Aoba, Aoba-Ku, Sendai 980-8578, Japan*

[c]*Department of Frontier Materials Chemistry, Graduate School of Science and Technology, Hirosaki University, 3 Bunkyo-cho, Hirosaki, 036-8561, Japan*

† These authors equally contributed to this work.

incorporating interlayer anions. These promising non-Ir OER catalysts often display higher OER activity than IrO_2 and have attracted the attention of a plethora of researchers; however, some controversial results regarding the stability of the catalyst have been reported. Some research groups have reported minimal reductions in the activity of NiFe-LDH during constant current operation at 10–100 mA cm^{-2} in a half cell employing 1 mol dm^{-3} KOH for 20 h[6] or at 1 A cm^{-2} in a single cell employing 1 mol dm^{-3} KOH for 50 h.[7] The Sun group reported a negligible degradation in current density of 2.2% after constant potential operation at 1.5 V *versus* a reversible hydrogen electrode (RHE) in a half cell employing 1 mol dm^{-3} KOH for 10 h.[8] In addition, Xie *et al.* reported a slight reduction in current density of 5.3% after holding at 1.6 V *versus* RHE for 5 h and a slight increase in overpotential after 4000 potential cycles, both conducted in a half cell employing 1 mol dm^{-3} KOH.[9] In these reports, NiFe-LDH catalysts were used without undergoing ion exchange processes to intercalate specific anions.[6–9] For these pure NiFe-LDH catalysts, other groups have reported contrasting results in terms of OER stability. The Guan group reported a clear loss in current density after constant potential operation at 1.5 V *versus* RHE for pure NiFe-LDH in 1 mol dm^{-3} KOH.[10] The Liu group reported that a local acidic environment within the interlayer of stacked pure NiFe-LDHs dissolved the nickel and iron to induce a gradual increase in overpotential at 500 mA cm^{-2} and 353 K over 20 h in a half cell employing 1 mol dm^{-3} KOH.[11] The delamination of stacked NiFe-LDH layers forming atomically thin layers has been reported to enhance the stability under those conditions significantly.[11] The Nicolosi group reported preferential leaching of iron at the OER active edge sites of NiFe-LDH and a subsequent reduction in its OER activity during the conditioning potential cycles in a half cell employing 1 mol dm^{-3} KOH.[5] The OER activity decreased continuously even after the cycle number was increased to 200, and the surface iron content decreased from 38.7 to 19 atomic% after 50 potential cycles.[5] These results from different research groups appear to conflict at first glance, indicating that pure NiFe-LDH is stable and unstable.

Other controversial results concern the active valences of nickel and iron. In cyclic voltammograms (CVs) of NiFe-LDH, redox peaks appear at approximately 1.3–1.4 V *versus* RHE in alkaline media, lower than the OER potential region of NiFe-LDH (above 1.5 V) and the oxidation (anodic) peak has been assigned to Ni^{2+} in $Ni(OH)_2$–Ni^{3+} in the NiOOH phase transition, similar to $Ni(OH)_2$.[8] The reduction (cathodic) peak has been assigned to the reverse valence/crystal phase transition.[8] Trotochaud *et al.* reported that $Ni(OH)_2$ and NiOOH are insulating and conductive, respectively, and incorporating iron increased the film conductivity of NiOOH by more than 30-fold.[12] In accordance with previous reports, several groups acknowledge that the Ni^{3+} in the NiOOH phase is the OER active site in NiFe-LDH.[7,9,13] Lei *et al.* reported surface reconstruction, *i.e.*, a phase transition of S-doped NiFe-LDH to S-doped Ni_x-Fe_yOOH with an increase in surface Ni^{3+} content during CVs, is the key to enhancing OER activity.[14] In previous reports, the Ni^{3+} in the NiOOH phase generated at high OER potential regions was reported to be active in OERs. In addition, higher nickel valences, such as $Ni^{4+}Fe^{3+}OOH$ (ref. 15) and $Ni^{4+}Fe^{4+}OOH$,[16] have been detected at high OER potentials using *in situ* X-ray absorption spectroscopy (XAS). In contrast, the active site was previously reported to be Fe^{3+}.[15] Görlin *et al.* reported different results by using *operando* differential electrochemical mass spectroscopy and quasi-*in situ* XAS. For the iron-free NiOOH catalyst, the oxidation state was Ni^{4+} at 1.63 V *versus* RHE in 0.1 mol dm^{-3} KOH, whereas Ni^{2+} was retained even at a high OER potential when the iron content exceeded 4 atomic% in $Ni_{1-x}{}^{2+}Fe_x{}^{3+}OOH$ catalysts.[17]

Studies reporting different stabilities and active sites in NiFe-LDH prompted us to investigate the stable valence states of pure NiFe-LDH. According to an intricate study by Görlin *et al.*,[17] Ni^{2+} should not be oxidized during the OER on NiFe-LDH if the catalyst is stable. Even when Ni^{2+} was converted into Ni^{3+} at a high OER potential, it should be reduced to Ni^{2+} after the OER if the redox reaction ($Ni^{2+} \leftrightarrow Ni^{3+} + e^-$) is reversible. However, more than half of Ni^{2+} on the surface of the as-prepared pure NiFe-LDH was converted into Ni^{3+} after only 40 CV cycles with an increased OER current based on the *ex situ* X-ray photoelectron spectroscopy (XPS) and electrochemical analyses conducted by Lei *et al.*[14] In addition, surface Ni^{2+} on as-prepared pure NiFe-LDH was reported to be converted into Ni^{3+} after stability tests[9] or initial activation processes.[13] As two contrasting results exist regarding the stability of pure NiFe-LDH, *i.e.*, stable or unstable, and certain reports do not assess the stability of NiFe-LDH, directly comparing these contrasting results on the stability of surface valence states is difficult. However, surface valence states are crucial in OERs because of their role in surface reactions. Therefore, the stabilities of surface valence states of pure NiFe-LDH, without doping or intercalation of specific anions, were investigated in this study.

Experimental section

Catalyst synthesis

A coprecipitation method for preparing a highly stable monolayer NiFe-LDH catalyst[7,18] was used with some modifications. First, 0.220 g of $Ni(NO_3)_2 \cdot 6H_2O$ (Fuji Film Wako Pure Chem. Co., Osaka, Osaka, Japan) and 0.107 g of $Fe(NO_3)_3 \cdot 9H_2O$ (Fuji Film Wako Pure Chem. Co., Osaka, Osaka, Japan) were dissolved in 20 cm^3 of distilled water by stirring in a polytetrafluoroethylene (PTFE) beaker that was placed in an aluminum bath filled with aluminum beads. The aluminum bath was set on a hot stirrer (RCH-20L, Eyela Co., Bunkyo-ku, Tokyo, Japan) and the temperature of the aluminum bath was controlled using a thermocouple connected to the stirrer. Second, 4.7 cm^3 of formamide (Fuji Film Wako Pure Chem. Co., Osaka, Osaka, Japan) was dissolved in 15.3 cm^3 of distilled water, and the formed formamide solution was added to the Ni/Fe solution under continuous stirring at room temperature. Third, a 0.25 mol dm^{-3} NaOH solution, which was prepared from NaOH pellets (Fuji Film Wako Pure Chem. Co., Osaka, Osaka, Japan) and distilled water, was added dropwise until the pH reached 10 with continuous stirring at room temperature. Finally, the temperature of the aluminum bath was increased to 353 K and held for 10 min, with continuous stirring using the

hot stirrer. After cooling, the solution was centrifuged at 10 000 rpm for 10 min using a centrifuge (LCX-100, Tomy Seiko Co., Nerima-ku, Tokyo, Japan) and washed with distilled water using a sonic stirrer (USS-1, Nihon Seiki Co., Katsushika-ku, Tokyo, Japan). The centrifugation and washing procedure was repeated three times to yield 200 cm^3 of NiFe-LDH solution. Half of the solution was placed into screw vials to prepare electrodes, and the remaining half was dried at 380 K in a convection oven for X-ray diffraction (XRD) pattern measurements.

For the preparation of LDHs with other metal combinations, $Mg(NO_3)_2 \cdot 6H_2O$ (Fuji Film Wako Pure Chem. Co., Osaka, Osaka, Japan) and/or $Al(NO_3)_3 \cdot 9H_2O$ (Fuji Film Wako Pure Chem. Co., Osaka, Osaka, Japan) were used.

Characterization

The bulk crystal structures of the catalysts were evaluated using an X-ray diffractometer (MiniFlex 600, Rigaku Co., Akishima, Tokyo, Japan) with Cu-Kα radiation generated at 40 kV and 15 mA (scan range = 20–80°, step size = 0.02°, and scan rate = 2° min^{-1}). The outermost surface and subsurface crystal structures of the NiFe-LDH catalysts were evaluated using a Raman spectrometer (Raman Force, Nanophoton Co. Ltd, Osaka, Japan) excited by ultraviolet (UV) (355 nm) and visible (532 nm) lasers, respectively. The morphology of the catalysts was investigated using a field emission scanning electron microscope (JSM-7000F, JEOL Inc., Akishima, Tokyo, Japan). The chemical/valence states of the catalysts were determined using an X-ray photoelectron (XP) spectrometer (PHI Quantera II, ULVAC-PHI, Inc., Chigasaki, Kanagawa, Japan) with an Al-Kα X-ray source (1486.6 eV). The peak shifts resulting from surface charges were corrected using the binding energy of C 1s (284.8 eV) of organic contaminants from the spectrometer and/or air. The Ni 2p and Fe 2p spectra were analyzed by fitting four and two symmetric peaks, respectively, after subtracting a Shirley-type background. As the contributions from the hydrocarbons and NiFe-LDH to the O 1s spectra cannot be distinguished, only Ni 2p and Fe 2p were used for these analyses.

OER activity and stability measurements

The OER activity and stability were measured using a conventional three-electrode PTFE cell with 1 mol dm^{-3} KOH solution. The working electrode was prepared by immersing Ni foam (NF, thickness: 1.6 mm, NI-318161, Nilaco Co., Chuo-ku, Tokyo, Japan) in the prepared catalyst solution overnight, which was then dried at 380 K in a convection oven (DKN302, Yamato Sci. Co., Chuo-ku, Tokyo, Japan). The NFs (dimensions 2 cm × 0.5 cm) were cleaned by sonication in 2 mol dm^{-3} HCl solution and distilled water, and then placed into an oven at 380 K before use. The catalyst-coated NF, hereafter denoted as NiFe-LDH/NF, a carbon rod (diameter: 5 mm, C-072591, Nilaco Co., Chuo-ku, Tokyo, Japan), and an Ag/AgCl (sat. KCl) electrode (HS-205C, TOA DKK Co., Shinjuku-ku, Tokyo, Japan) were used as the working, counter, and reference electrodes, respectively. All potentials were referenced to an RHE. After bubbling O_2 for more than 1800 s, the CVs were recorded from 1.1 V to 1.7 V of applied potential, E_w, at a scan rate of 5 mV s^{-1} for 20 cycles to reach a steady state, using a potentiostat (PGSTAT204, Autolab Co., Utrecht, Utrecht, Netherlands) to evaluate the OER activity. Nyquist plots were measured by applying a root mean square alternating current voltage at 10 mV in the frequency range from 100 mHz to 100 kHz at 1.5 V *versus* the RHE. The solution resistance between the working electrode and reference electrode, R, was determined using the high-frequency intercept of the Nyquist plots, and all the potential values were corrected by $E = E_w - IR$ where I is the measured current.

In situ Raman spectroscopy was performed to investigate the changes in subsurface crystal structure at various E using a specially designed cell. The cell was made of polychlorotrifluoroethylene (PCTFE) with a sapphire window for *in situ* measurements, and three electrode holders for a visible Raman spectrometer (iHR320, Horiba Scientific Co. Ltd, Kyoto, Kyoto, Japan). The working electrode was prepared by pipetting NiFe-LDH solution onto a Ni rod, which was then dried at 380 K in a convection oven. The counter and reference electrodes were a Pt wire and a homemade Ag/AgCl (sat. KCl) electrode, respectively. For *in situ* Raman spectroscopic measurements, an argon ion laser (Innova 70, Coherent, Inc., U.S.A., 514.5 nm, 100 mW) was focused on the surface of the working electrode with a spot size of 0.13 × 1.3 mm^2. The angle of incidence of the beam was about 60° at the electrode surface. We utilized the large spot size to avoid thermal damage from the laser beam while allowing efficient light collection for the spectrometer. The effective area of the electrode in contact with the electrolyte was 0.21 cm^2. The scattered light from the electrode surface was transmitted through the sapphire window of the electrochemical cell, collected by an achromatic lens, and focused on the entrance slit of the single-stage spectrometer. Raman spectra were recorded every 50 mV from the OCP with 100 seconds of data accumulation. Generally, we took several tens of *in situ* Raman spectra for one sample in one go. All the Raman spectra are averaged over multiple measurements.

Results and discussion

In previous reports using the coprecipitation method,[7,18] NiFe-LDH catalyst "inks" were prepared by mixing the catalyst with isopropyl alcohol or ethanol-based solvents. Then, the ink was coated on glassy carbon[7] or graphite paper[18] to evaluate the OER activity in half cells. In this study, NiFe-LDH was directly coated on NF by immersing the NF in a NiFe-LDH solution. Fig. 1(a) and (b) show field emission scanning electron microscopy (FE-SEM) images of NF and NiFe-LDH/NF, respectively. The open structure of the NF was successfully retained after coating with NiFe-LDH. In addition, the open structure was retained regardless of the metal combination used for the LDH (Fig. S1, SI), indicating that the coating method in this study does not change the pore structure of the NF, which will enable the rapid transport of OH^- and O_2 gas generated during the OERs. Fig. 1(c) shows an XRD pattern of the NiFe-LDH powder obtained by drying the NiFe-LDH solution at 380 K. All peaks derived from the powder were assigned to pure NiFe-LDH with the chemical formula $Ni_{0.75}Fe_{0.25}(OH)_2(CO_3)_{0.125} \cdot 0.38H_2O$

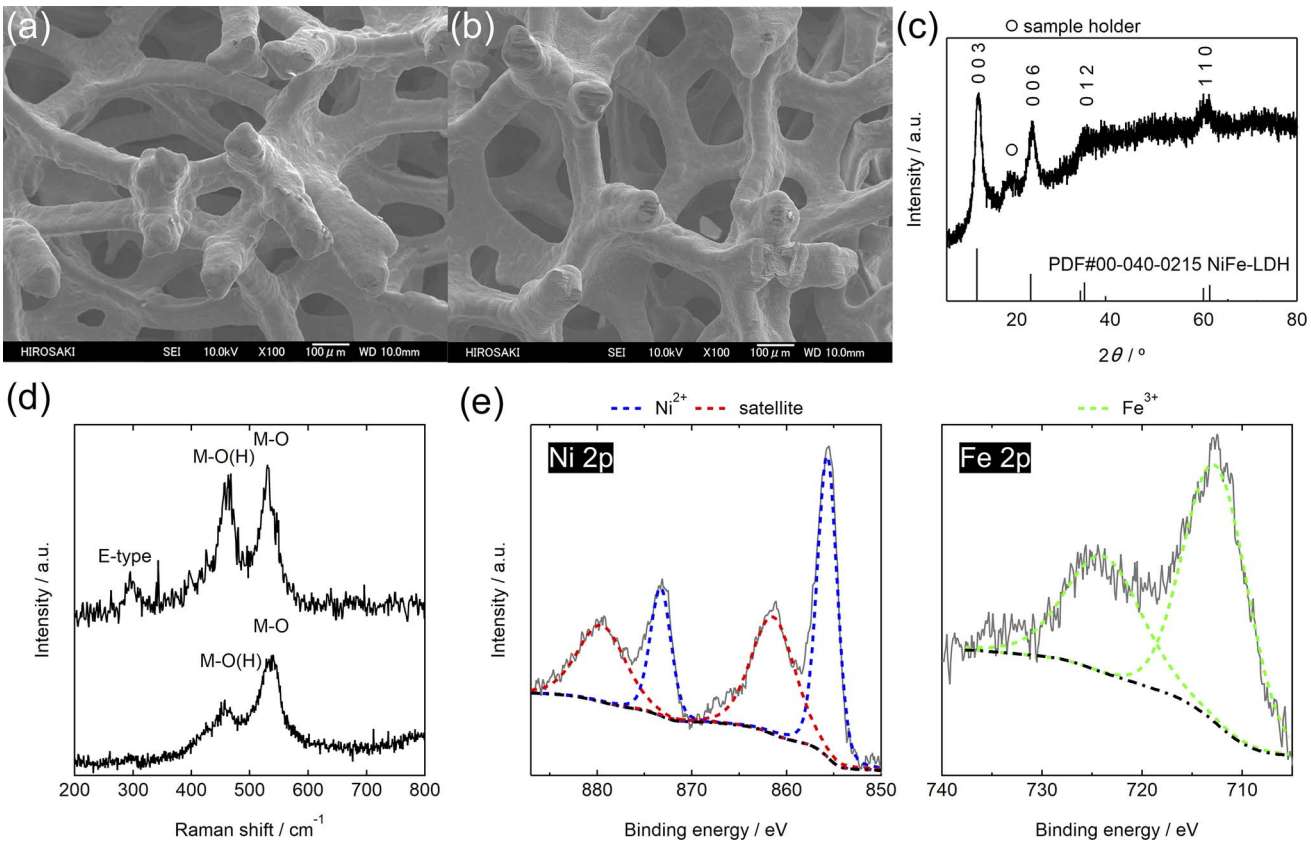

Fig. 1 Field emission-scanning electron microscopy (FE-SEM) images of (a) nickel foam (NF) and (b) nickel–iron layered double hydroxide on NF (NiFe-LDH/NF). (c) X-ray diffraction (XRD) pattern, (d) (bottom) visible and (top) ultraviolet (UV) Raman spectra, and (e) Ni 2p (left) and Fe 2p (right) X-ray photoelectron (XP) spectra of NiFe-LDH.

(powder diffraction file number 00-040-0215), in agreement with the reports by Jeon *et al.* in which monolayer stacking proceeded during drying at 333 K, resulting in similar XRD peaks.[7] The origin of the interlayer CO_3^{2-} anion is carbon dioxide gas from the air during preparation.[5] The powder XRD pattern reveals the phase purity of the synthesized NiFe-LDHs in bulk. The surface crystal structure was investigated using Raman spectroscopy excited with visible and UV laser irradiation at 532 and 355 nm, respectively. Certain oxide materials, such as TiO_2 and ZrO_2, absorb UV light strongly; therefore, UV Raman spectroscopy displays increased surface sensitivity compared with visible Raman for these types of materials.[19,20] The effect of laser wavelength on the Raman spectra of the NiFe-LDH films formed on the Ni rods is displayed in Fig. 1(d). The visible Raman spectrum displayed two broad peaks at ~461 cm^{-1} and ~533 cm^{-1}, assigned to the M^{2+}–O(H) and M^{2+}–O vibration modes of NiFe-LDH, respectively.[21–23] Comparing these two peaks in the visible and UV Raman spectra, their full width at half maximum was lower and displayed sharpened peaks in the UV spectrum. In addition, a small but distinct peak appeared at ~296 cm^{-1} that was assigned to the E-type vibration mode of NiFe-LDH.[22,23] These results indicate that the outermost surface had a higher degree of crystallinity than the subsurface. Furthermore, the UV Raman spectrum displayed a peak at ~343 cm^{-1} that is absent in the corresponding visible Raman spectrum. This study is the first to report the UV Raman spectrum of NiFe-LDH, and similar peaks were not observed in previous papers reporting the visible Raman spectra of NiFe-LDH;[21–23] therefore, assigning the peak at ~343 cm^{-1} is currently not possible. Future studies with other spectroscopic analyses are necessary to assign the ~343 cm^{-1} peak that is present only on the outermost surface. The surface chemical/valence states of NiFe-LDH evaluated using XPS are shown in Fig. 1(e). The Ni 2p level splits into Ni $2p_{3/2}$ and $2p_{1/2}$ sublevels to display doublets at two unique binding energies. The peaks at ~855 and ~873 eV are assigned to Ni^{2+} in NiFe-LDH, and the broader peaks at ~862 and ~880 eV are assigned to the satellite peaks.[9,14] The Fe 2p level also splits into Fe $2p_{3/2}$ and $2p_{1/2}$ sublevels, showing peaks at ~713 and ~725 eV that are assigned to Fe^{3+} in NiFe-LDH.[9,14] The results displayed in Fig. 1(a)–(e) indicate that $Ni^{2+}Fe^{3+}$-LDHs were formed on the NF, and that the open pore structure was maintained.

Fig. 2(a) displays the OER activity of four LDHs, $[M1_{0.75}{}^{2+}M2_{0.25}{}^{3+}(OH)_2]^{x+}(A^{n-})_{x/n}\cdot y(H_2O)$ where M1 = Ni, Mg, M2 = Fe, Al. The M1/M2 atomic ratio was optimized for the OER activity of the NiFe-LDH series and set to 3 (Fig. S2, SI). This ratio was used to prepare other combinations of M1/M2 metals in the LDHs. The NiFe-LDH/NF exhibited the highest OER activity among the four catalysts, indicating that the combination of Ni^{2+} and Fe^{3+} was the optimal selection among these

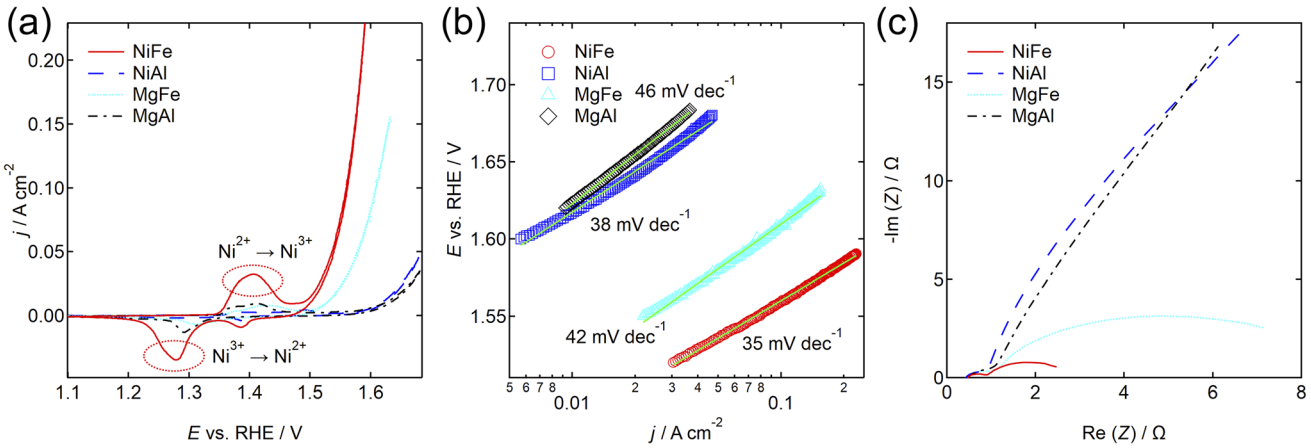

Fig. 2 (a) Cyclic voltammograms (CVs), (b) Tafel plots, and (c) Nyquist plots of NiFe-LDH/NF, NiAl-LDH/NF, MgFe-LDH/NF, and MgAl-LDH/NF in O_2-saturated 1 mol dm^{-3} KOH. The scans were performed at a scan rate of 5 mV^{-1} in (a) and (b).

catalyst series. Notably, the anodic peak at ~1.4 V, indicated with a dashed circle in Fig. 2(a), originates from the oxidation of Ni from Ni^2 to Ni^{3+} rather than the OER, and the cathodic peak at ~1.3 V results from the reverse reaction.[7–9] The overpotential required to yield 10 mA cm^{-2} of geometrical current density, j, from NiFe-LDH/NF, was 257 mV, similar to that reported for a monolayer NiFe-LDH formed on a glassy carbon electrode (250 mV)[7] and on graphite paper (272 mV).[18] Thus, the coprecipitation method developed by these authors[7,18] was successfully applied to NF in this study without forming catalyst powders and catalyst inks. The method could be applied to prepare other LDHs; however, the OER activities were lower than with NiFe-LDH/NF. In addition, the NiFe-LDH displayed the lowest Tafel slope (35 mV dec^{-1}) among the four synthesized catalysts, as shown in Fig. 2(b). Aligning with these results, NiFe-LDH displayed the smallest semicircles in the Nyquist plots shown in Fig. 2(c), indicating the lowest charge transfer resistance.

The stability of NiFe-LDH/NF was evaluated using a chronopotentiometry (CP) until a preset time, t, of 24 h was reached. Fig. 3(a) shows the E–t plot and Fig. 3(b) shows the CV plots before and after 24 h of CP for NiFe-LDH/NF. The E value remained almost unchanged at $j = 0.05$ A cm^{-2} during the CP experiment, and the CVs changed minimally in the OER region at $E > 1.5$ V, indicating that the OER activity of NiFe-LDH/NF remained unchanged, similar to previous work conducted by Jeon *et al.*[7] Although the source of this stability is beyond the scope of this paper, it could result from the monolayer structure of NiFe-LDH produced *via* the coprecipitation method used in this study.[7,18] Previously, atomically thin layers have been reported to be stable and avoid dissolution in local acidic environments because of the stacked NiFe-LDHs.[11] The CVs at $E \leq 1.5$ V changed a little; both the anodic peak at ~1.4 V and cathodic counterpart at ~1.3 V slightly shifted positively by 0.01 V after the CP, as shown in Fig. 3(b). The precise mechanism for these slight changes in the redox peak potentials is not clear at this stage. However, one of the reasons could be the change in the local OH^- concentration. Because OH^- ions were consumed to produce water during the OER ($4OH^- \rightarrow O_2 + 2H_2O + 4e^-$) in the half cell, the local OH^- concentration on the surface of NiFe-LDH/NF should decrease. Both the anodic and cathodic peak potentials have been reported to increase with decreasing KOH concentration.[24,25] Therefore, both anodic and cathodic peak potentials of NiFe-LDH/NF increased after 24 h of CP. As noted earlier, the anodic peak at ~1.4 V in the CVs was assigned to the change in the valence state of Ni, Ni^{2+} to Ni^{3+} and the cathodic counterpart at ~1.3 V as the reverse reaction, Ni^{3+} to Ni^{2+}.[7–9] The CVs shown in Fig. 3(b) indicate that the Ni valence state was 2+ after the CP as E returned to 1.1 V during the OER activity measurements. Then, the surface stability was evaluated using XPS, and the results are shown in Fig. 3(c). The Ni 2p and Fe 2p spectra changed minimally, and Ni^{2+} and Fe^{3+} were retained on the surface of NiFe-LDH/NF. These results indicate that the surface of the NiFe-LDH/NF was stable and resistant to changes in the initial valence states of Ni^{2+} and Fe^{3+}, at least during the stable operation period. The results are consistent with the CVs shown in Fig. 3(b) and do not preclude the production of higher valence states, such as Ni^{3+} or Fe^{4+}, during the OER reported earlier.[14,16] The changes in the surface crystal structure during the OER were investigated using *in situ* visible Raman spectroscopy with excitation from a 514.5 nm laser, as shown in Fig. 4(a). In 1 mol dm^{-3} KOH solution, NiFe-LDH displayed only two peaks, originating from the Ni^{2+}–O(H) and Ni^{2+}–O vibration modes at open circuit potential (OCP), similar to the visible Raman spectrum of NiFe-LDH measured in air, shown in Fig. 1(d). The spectra did not change significantly with an increase in E to 1.325 V, whereas two new peaks appeared at ~474 and ~555 cm^{-1} when $E = 1.375$ V indicating the oxidation of Ni from $Ni^{2+}(OH)_2$ to $Ni^{3+}OOH$ in NiFe-LDH,[21–23] aligning with the CV results obtained in a PTFE cell where the Ni^{2+} to Ni^{3+} transition was observed *via* the anodic peak at ~1.4 V in Fig. 2(a). The PCTFE cell used for *in situ* Raman spectroscopy differs from the PTFE cell used for OER activity measurements. However, the Ni^{2+} to Ni^{3+} transition proceeded at a similar E value of ~1.4 V; thus, the measured potential was well calibrated between these two cells. The two oxyhydroxide peaks grew while their hydroxide counterparts deteriorated with an increase in E up to 1.475 V. When E

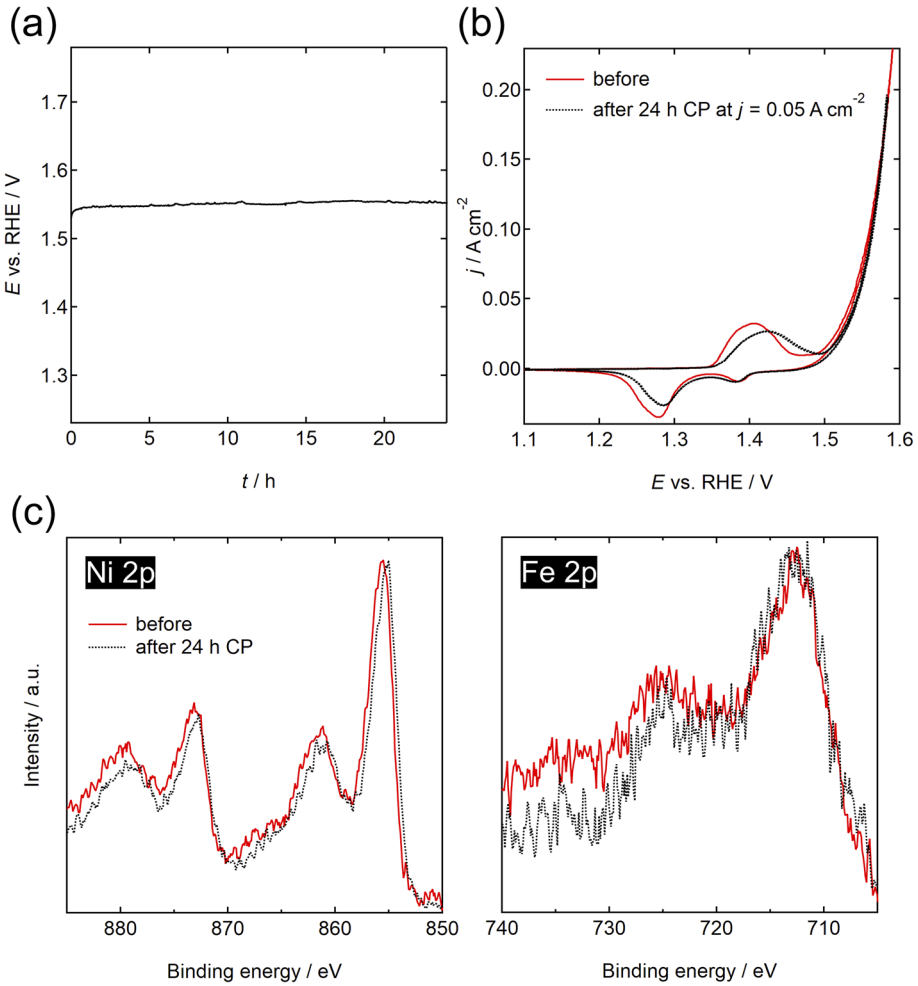

Fig. 3 (a) Potential *versus* time (*E*–*t*) curve of NiFe-LDH/NF during chronopotentiometry (CP) at a constant current density, $j = 0.05$ A cm^{-2}. (b) CV plots, (c) XP Ni 2p and Fe 2p spectra of NiFe-LDH/NF before (solid curves) and after (dashed curves) 24 h of CP at $j = 0.05$ A cm^{-2}.

exceeded 1.5 V, OER proceeded, and the NiOOH-derived peaks broadened, indicating the defective nature of these reaction conditions. Thus, the OER active oxyhydroxides contained defects, including oxygen and cation vacancies. These results do not preclude the presence of metals with valences that are higher than the metal in a stoichiometric oxyhydroxide ($M^{3+}OOH$), such as $Ni^{4+}Fe^{3+}OOH$,[15] $Ni^{4+}Fe^{4+}OOH$,[16] or amorphous $Ni^{4+}O_x$.[21] The charge imbalance resulting from the higher metal valence in the oxyhydroxides could be compensated for by inserting interlayer anions and/or incorporating cation vacancies. The small cathodic peak at ~1.4 V in the CV of NiFe-LDH/NF shown in Fig. 2(a) could be assigned to the reduction of Ni^{4+} to Ni^{3+}; however, detecting such tetravalent cations should be accomplished with other techniques because Raman spectroscopy does not directly measure metal valances. Raman spectra could be measured at $E \leq 1.550$ V but the large amount of O_2 gas evolved by the OER precluded measurement of the spectra at $E > 1.550$ V. At the highest measured *E* value (1.550 V), a small $Ni(OH)_2$ peak at 523 cm^{-1} remained, indicating the incomplete conversion of hydroxides to oxyhydroxides. Then, the *E* value was decreased to OCP to elucidate the reversibility of the surface crystal structure, as shown in Fig. 4(b). The NiOOH peaks sharpened slightly, whereas the small $Ni(OH)_2$ peak at 523 cm^{-1} diminished with a decrease in *E* to the OCP, indicating that oxyhydroxides were not reconverted into hydroxides after exposure to high OER potentials. At each *E*, the spectrum was measured for 100 seconds. The hydroxides could be converted into oxyhydroxides during the long measurement period even at $E \leq 1.550$ V. Compared with the initial hydroxide peaks at the OCP before applying potential, shown at the bottom of Fig. 4(a), the oxyhydroxide peaks at OCP after cycling the potential shown at the bottom of Fig. 4(b) are broader, indicating the presence of a plethora of defects in the oxyhydroxides. The irreversible surface crystal structure changes investigated using *in situ* Raman spectroscopy (Fig. 4) and the reversible valence states evaluated using *ex situ* XPS (Fig. 3(c)) indicate that the initial hydroxide crystal structure in $Ni^{2+}Fe^{3+}$-LDH was converted into an oxyhydroxide structure after the first OER test. Both the CVs displaying a cathodic peak at ~1.3 V in Fig. 3(b) and the XP spectra displayed in Fig. 3(c) indicate that the valence states could be converted back to Ni^{2+} and Fe^{3+} even after a 24 h stability test. From the XRD (Fig. 1(c)), XPS (Fig. 3(c)) and *in situ* Raman spectroscopy (Fig. 4) analyses, the chemical formula of

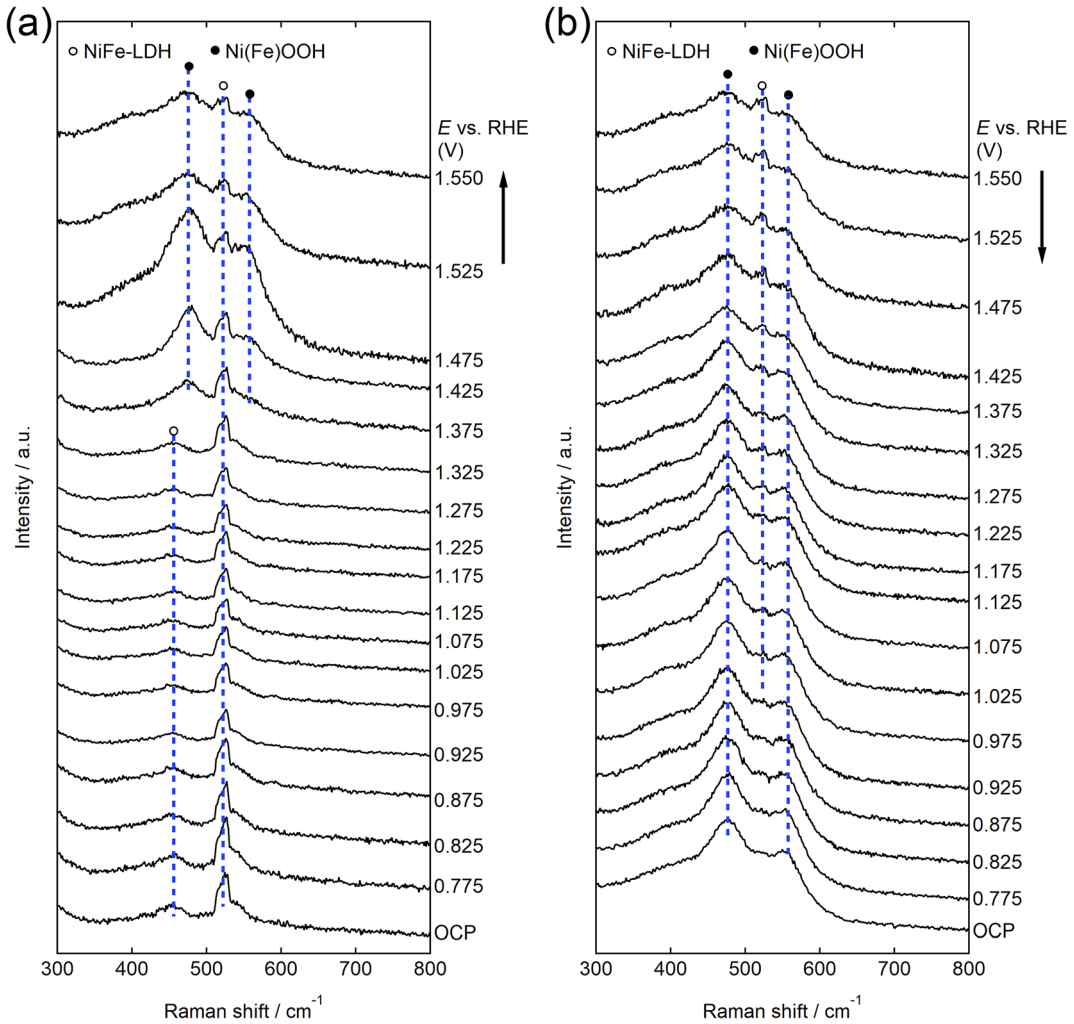

Fig. 4 *In situ* visible Raman spectra of a NiFe-LDH/Ni rod during (a) an increase in *E* from open circuit potential (OCP) to 1.550 V and (b) a decrease in *E* from 1.550 V to OCP in O_2-saturated 1 mol dm^{-3} KOH.

the as-prepared NiFe-LDH is $[Ni_{0.75}{}^{2+}Fe_{0.25}{}^{3+}(OH)_2]^{0.25+}$-$(CO_3{}^{2-})_{0.125}\cdot 0.38(H_2O)$ and the formula after the OER tests is $[Ni_{0.75}{}^{2+}Fe_{0.25}{}^{3+}OOH]^{0.75-}(CO_3{}^{2-})_{0.125}\cdot 0.38(H_2O)$ if the oxyhydroxide contained no defects. Therefore, a charge imbalance (-1) is created in the oxyhydroxide without defects. Potentially, the charge imbalance in the oxyhydroxide was compensated for by incorporating oxygen vacancies and releasing interlayer anions to form $[Ni_{0.75}{}^{2+}Fe_{0.25}{}^{3+}O_{1-x}OH]^{(0.75-2x)-}$-$(CO_3{}^{2-})_{0.125-y}\cdot 0.38(H_2O)$. For example, the charge is balanced when $x = 0.475$ and $y = 0.025$. Therefore, the reversible valence states shown in Fig. 3 agree with the irreversible crystal structures indicated by the Raman spectra shown in Fig. 4. Regardless of whether the surface was converted to high valence(s) Ni^{3+}, Ni^{4+}, or Fe^{4+} during OER, the initial valence states of Ni^{2+}/Fe^{3+} were recovered after OER when the NiFe-LDH displayed stable performance.

Conclusions

The stability of the surface of stable NiFe-LDH was investigated using *in situ* visible Raman spectroscopy, *ex situ* visible/UV Raman spectroscopy, *ex situ* XPS, and CP in alkaline media. Although previous reports describe significant changes in the surface valence states for pure NiFe-LDH during OERs, in this study, we prepared a stable pure NiFe-LDH on NF using a recently reported coprecipitation method, and the surface Ni^{2+} and Fe^{3+} remained unchanged during the 24 h of CP measurements. *Insitu* Raman spectroscopy revealed that the surface crystal structure underwent an irreversible change from hydroxides to oxyhydroxides after the OER. However, the stable valence states revealed by *ex situ* XPS indicate that the Ni^{2+}/Fe^{3+} valences were reversible during OER even if the valences increased at high potentials. The charge imbalance in oxyhydroxides with Ni^{2+}/Fe^{3+} was potentially compensated for by incorporating oxygen vacancies and releasing interlayer anions. The defective nature of surface oxyhydroxides after OER revealed by *in situ* Raman spectroscopy supports the presence of oxygen vacancies. Although changes in Ni/Fe valence during unstable NiFe-LDH operations have been reported, our results clearly indicate that the valence remained unchanged for stable NiFe-LDH. The key difference between this study and previous reports in which unstable NiFe-LDH was presented is

potentially the monolayer structure produced by the coprecipitation method used in this study. Our next research will examine the stability of NiFe-LDHs with specific intercalated anions, which could enhance the OER activity.

Author contributions

Taiyo Fukui worked on conceptualization and investigation. Takashi Itoh worked on investigation, resources, formal analyses, validation, writing – review and editing. Mitsuharu Chisaka worked on data curation, supervision, resources, formal analyses, writing – original draft, writing – review and editing, funding acquisition. Toshiyuki Abe worked on validation, writing – review and editing.

Conflicts of interest

There are no conflicts to declare.

Data availability

Data associated with the results of this article are available as part of the main text, and data supporting this article have been included as part of the SI.

FE-SEM images, CVs. See DOI: **https://doi.org/10.1039/d5su00578g**.

Acknowledgements

The authors acknowledge Yusei Tsushima, affiliated to Hirosaki University, for acquiring the FE-SEM images. This work was partially supported by a Grant-in-Aid for Scientific Research, Grant Number JP23K26042 from the Ministry of Education, Culture, Sports, Science and Technology (MEXT) in Japan.

References

1 T. Ahmad and D. Zhang, *Energy Rep.*, 2020, **6**, 1973.
2 U.S. Geological Survey, *Miner. Commod. Summ.*, 2024, 136, DOI: **10.3133/mcs2024**.
3 K. Zeng and D. Zhang, *Prog. Energy Combust. Sci.*, 2010, **36**, 307.
4 F. Dionigi and P. Strasser, *Adv. Energy Mater.*, 2016, **6**, 1600621.
5 D. Tyndall, M. J. Craig, L. Gannon, C. McGuinness, N. McEvoy, A. Roy, M. García-Melchor, M. P. Browne and V. Nicolosi, *J. Mater. Chem. A*, 2023, **11**, 4067.
6 S. H. Kim, Y. S. Park, C. Kim, I. Y. Kwon, J. Lee, H. Jin, Y. S. Lee, S. M. Choi and Y. Kim, *Energy Rep.*, 2020, **6**, 248.
7 S. S. Jeon, J. Lim, P. W. Kang, J. W. Lee, G. Kang and H. Lee, *ACS Appl. Mater. Interfaces*, 2021, **13**, 37179.
8 Z. Lu, W. Xu, W. Zhu, Q. Yang, X. Lei, J. Liu, Y. Li, X. Sun and X. Duan, *Chem. Commun.*, 2014, **50**, 6479.
9 J. Xie, H. Qu, F. Lei, X. Peng, W. Liu, L. Gao, P. Hao, G. Cui and B. Tang, *J. Mater. Chem. A*, 2018, **6**, 16121.
10 X. Li, X. Hao, Z. Wang, A. Abudula and G. Guan, *J. Power Sources*, 2017, **347**, 193.
11 R. Chen, S. F. Hung, D. Zhou, J. Gao, C. Yang, H. Tao, H. B. Yang, L. Zhang, L. Zhang, Q. Xiong, H. M. Chen and B. Liu, *Adv. Mater.*, 2019, **31**, 1903909.
12 L. Trotochaud, S. L. Young, J. K. Ranney and S. W. Boettcher, *J. Am. Chem. Soc.*, 2014, **136**, 6744.
13 C. Qiao, Z. Usman, T. Cao, S. Rafai, Z. Wang, Y. Zhu, C. Cao and J. Zhang, *Chem. Eng. J.*, 2021, **426**, 130873.
14 H. Lei, L. Ma, Q. Wan, S. Tan, B. Yang, Z. Wang, W. Mai and H. J. Fan, *Adv. Energy Mater.*, 2022, **12**, 2202522.
15 D. Friebel, M. W. Louie, M. Bajdich, K. E. Sanwald, Y. Cai, A. M. Wise, M. J. Cheng, D. Sokaras, T. C. Weng, R. Alonso-Mori, R. C. Davis, J. R. Bargar, J. K. Nørskov, A. Nilsson and A. T. Bell, *J. Am. Chem. Soc.*, 2015, **137**, 1305.
16 D. Wang, J. Zhou, Y. Hu, J. Yang, N. Han, Y. Li and T. K. Sham, *J. Phys. Chem. C*, 2015, **119**, 19573.
17 M. Görlin, P. Chernev, J. Ferreira de Araújo, T. Reier, S. Dresp, B. Paul, R. Krähnert, H. Dau and P. Strasser, *J. Am. Chem. Soc.*, 2016, **138**, 5603.
18 X. Zhang, Y. Zhao, Y. Zhao, R. Shi, G. I. N. Waterhouse and T. Zhang, *Adv. Energy Mater.*, 2019, **9**, 1900881.
19 J. Zhang, M. Li, Z. Feng, J. Chen and C. Li, *J. Phys. Chem. B*, 2006, **110**, 927.
20 M. Li, Z. Feng, G. Xiong, P. Ying, Q. Xin and C. Li, *J. Phys. Chem. B*, 2001, **105**, 8107.
21 M. Liu, K. Min, B. Han and L. Y. S. Lee, *Adv. Energy Mater.*, 2021, **11**, 2101281.
22 S. Zhou, H. He, J. Li, Z. Ye, Z. Liu, J. Shi, Y. Hu and W. Cai, *Adv. Funct. Mater.*, 2024, **34**, 2313770.
23 S. Jung, R. A. Senthil, A. Min, A. Kumar, C. J. Moon, G. H. Jeong, T. W. Kim and M. Y. Choi, *J. Mater. Chem. A*, 2024, **12**, 8694.
24 S. Dresp, F. Dionigi, M. Klingenhof, T. Merzdorf, H. Schmies, J. Drnec, A. Poulain and P. Strasser, *ACS Catal.*, 2021, **11**, 6800.
25 S. A. Patil, P. B. Jagdale, N. Barman, A. Iqbal, A. Sfeir, S. Royer, R. Thapa, A. K. Samal and M. Saxena, *J. Colloid Interface Sci.*, 2024, **674**, 587.